Investigation of optical, electrical and magnetic properties of Tb-doped ZnO nanorods

Nupur Aggarwal[1] · Ajay Vasishth[1] · Kamaldeep Kaur[2] · N. K. Verma[2]

Abstract

The hydrothermally synthesised nanorods of $Zn_{1-x}Tb_xO$ (x = 0.00, 0.02, 0.05, 0.1) were carried over here to analyse the changes in its optical, magnetic and electrical behavior on doping. Formation of hexagonal wurtzite structure with particle size in the range of 36 nm–22 nm was confirmed by X-Ray diffraction studies. The morphology of the samples was confirmed by SEM (Scanning electron microscope) images alongwith its TEM (transmission electron microscope) micrographs. SAED (Selected area electron diffraction) and HRTEM (High resolution transmission electron microscope) shows the clear formation of nanorods. The quantitative analysis of elemental composition was done by energy dispersive X-ray spectroscopy (EDAX). The effect of increase in dopant concentration on band gap was analysed by UV-vis spectra; the band gap was found to be 3.35, 3.31, 3.30, 3.28 eV for undoped and 2%, 5% and 10% Tb-doped ZnO nanorods respectively. The presence of various types of defects was verified by PL study. The room temperature ferromagnetism behavior was tested by VSM and saturation magentization varies from 0.004 emu/g to 0.05 emu/g for undoped to 10% tb-doped ZnO nanorods. The dependence of resistivity on dopant concentration was carried out by four probe method which shows rise in resistivity with increasing dopant concentration.

1 Introduction

In the last few years metal oxides, such as Zinc oxide (ZnO), have sought interest of various researchers because of their less toxic nature and low cost. The usage of zinc oxide has been seen as a feasible way out for environmental protection [1]. ZnO in its hexagonal wurtzite form have a direct band gap value of 3.37 eV with a high exciton binding energy (~60 meV) at room temperature [2]. A wide range of applications of ZnO include field-effect transistor, optical device, dye-sensitized solar cell, solid-state gas sensor etc. [3–5]. ZnO semiconductors show n- type behavior as electrons act as charge carriers in conduction band. Various applications of ZnO are based on its composition along with some important properties such as grain size, density and morphology [6]. In the previous reports the doping of transition metal ions introduces RTFM in ZnO lattice. This RTFM behavior in ZnO arises due to presence of partially filled 3d shells of TM metal ions. But TM doped ZnO offers smaller magnetic moment as compare to RE dopant ions [7]. The presence of partially filled 4f orbital results in ferromagnetic ordering which results in larger magnetic moment and enhanced RTFM behavior of RE metal doped ZnO samples [8–10]. Terbium (Tb) possesses high magnetic moment per atom (9μB), which makes it a good dopant material as compared to transition metals having low magnetic moment. Alongwith this extraordinary optical property of Tb makes Tb-doped ZnO DMS material significant for not only magnetic study but also for magneto-optical and optoelectronic devices [11]. The work on influence of dopant on physical, optical, magnetic and electrical properties of ZnO is concerned with its applications in various magnetic devices and electronic component.

In present work, our aim is to synthesis Tb-doped ZnO nanorods in order to increase its magnetization at room temperature and its optical and electrical behavior is also analyzed. It is evident from the results that variation of dopant concentration helps in modifying behavior of ZnO nanomaterials to make it more suitable for DMS based applications.

✉ Nupur Aggarwal
nupurmittal09@gmail.com

1 Department of Physics, Chandigarh University, Gharuan, Mohali, India

2 School of Physics and Materials Science, Thapar Institute of Engineering and Technology, Patiala, India

2 Experimental

Various concentration of $Zn_{1-x}Tb_xO$ (x = 0.00, 0.02, 0.05 and 0.1) nanorods were prepared by conventional hydrothermal method. The synthesis procedure of nanorods is same as given in the literature [12, 13]. Zinc acetate dihydrate: $(Zn(CH_3COO).2H_2O)$ and Terbium (III) nitrate pentahydrate: $(Tb(NO_3)_3.5H_2O)$ procured from sigma Aldrich (~99% purity) were used as a precursors of Zinc and Terbium respectively. Firstly, stoichiometric measure of CTAB and NaOH were mixed in 50 mL of refined water and then freeze it for 15 min. 5.95 g of Zinc nitrate hexahydrate $[Zn(NO_3)_2.6H_2O]$ was made to dissolve in 50 mL of water accompanied by irresistible stirring at normal room temperature. The deep-freeze mixture of CTAB and NaOH is then combined with Zinc nitrate solution and mixed for 60 min on stirrer. This arrangement is then moved in 100 ml Teflon coated stainless steel autoclave and maintained at 200 °C for 20 h. To finish all the precipitates, which were obtained by the centrifugal method are usually dried approximately at 80 °C to acquire ZnO nanorods. Similar method was opted for various concentrations of Tb-doped ZnO nanorods.

The structural analysis of prepared samples was done by using (PANalytical X'Pert PRO MRD) X-ray Diffractometer with C_u-K_α ($\lambda = 1.5406$ Å) operated at 45 kV and 40 mA in the range of $20° \leq \theta \leq 80°$. The formation of rod-like structure was confirmed with the help of (Hitachi-H7650) high resolution transmission electron microscope (HRTEM). The quantitative elemental composition analysis was carried out by energy dispersive X-ray spectroscopy (EDAX) system of OXFORD analytical. *Perkin Elmer Lambda 45 spectrophotometer* in the wavelength range of 200–800 nm was used to obtain UV-Vis absorption spectrum and *Perkin Elmer*

fluorescence spectrometer was used to find PL spectrum with excitation wavelength of 310 nm to analyze the optical behavior of ZnO nanorods. The M–H plot of synthesized nanorods was recorded by Lake Shore's fully integrated vibrating sample magnetometer (Lake Shore model-7404). The resistivity measurement was done with four probe arrangement.

2.1 Structural study

The crystallinity and crystal orientation of the undoped and Tb-doped ZnO nanorods are indicated in their respective XRD pattern (Fig. 1). In diffraction pattern the peak position of the synthesized samples are in accordance with the hexagonal wurtzite structure of ZnO indicated in standard JCPDS card no 36-1451 [8]. Absence of any additional peak indicates the purity of samples and successful substitution of Tb ions inside the host material. Furthermore, the intensity of the peaks gets reduced with increasing dopant concentration exhibiting decrease in crystallinity of nanorods on doping [14].It has been observed that diffraction patterns exhibit broad peaks showing that the synthesized nanorods are composed of smaller crystallites [15].

To find the effect of dopant on the crystallite size of ZnO nanorods, Scherrer's formula was used as given here:

$$D = \frac{0.9\lambda}{\beta\cos\theta}$$

where, D is the size of crystal; λ, the wavelength; β, is the line broadening at half of the value of maximum intensity (FWHM) and, θ, the diffraction angle [16, 17]. The calculated values of crystallite size and lattice parameters were reported in Table 1. Figure 1 confirms no impurity phase

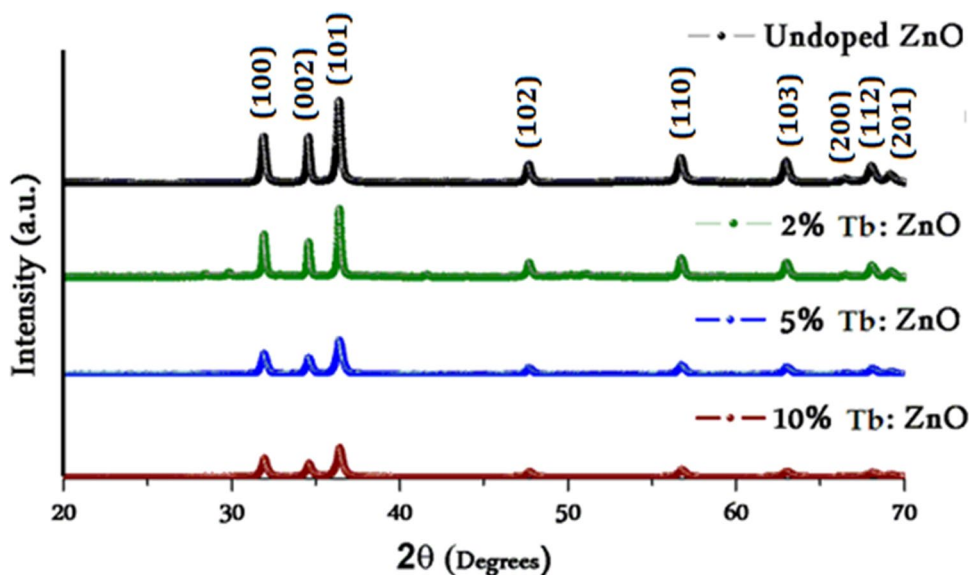**Fig. 1** XRD pattern of undoped and Tb (0.02, 0.05 and 0.10) doped ZnO nanorods

Table 1 Values of lattice parameters, d-spacing, crystallite size, band gap, and saturation magnetization for undoped and Tb-doped ZnO nanorods

Doping concentration (% age)	Lattice parameters		d-spacing (nm)	Crystallite size (nm)	Band gap (eV)	Saturation magnetization (emu/g)
	a = b (Å)	c (Å)				
0.00	3.246	5.175	2.472	36.71	3.35	0.0042
0.02	3.244	5.185	2.471	30.02	3.31	0.0276
0.05	3.231	5.187	2.463	23.90	3.30	0.0359
0.10	3.229	5.201	2.462	22.59	3.28	0.0519

evident in Tb-doped ZnO samples, specifies that the prepared samples are of single phase which clearly indicates that Terbium has been incorporated into the lattice properly.

2.2 Morphological and compositional study

Figure 2 (a-d) represent the images of SEM, SAED, TEM and HRTEM respectively of the Tb-doped ZnO nanorods, which confirm the rod like morphology of the samples. SEM image as well as TEM micrograph confirms the

formation of rod-like morphology of the synthesized sample. The presence of clear fringes has been observed in HRTEM analysis and the observed value of d-spacing is 0.357 nm. The diameter of the nanorods lies in between 40 and 50 nm. The chemical composition of 10% Tb-doped ZnO nanorods was analyzed by using EDAX spectra. Figure 3 confirms that synthesized nanorods were composed of Zn, Tb and O and are in accordance of their stoichiometry. Also it ensures the absence of any kind of impurity ions.
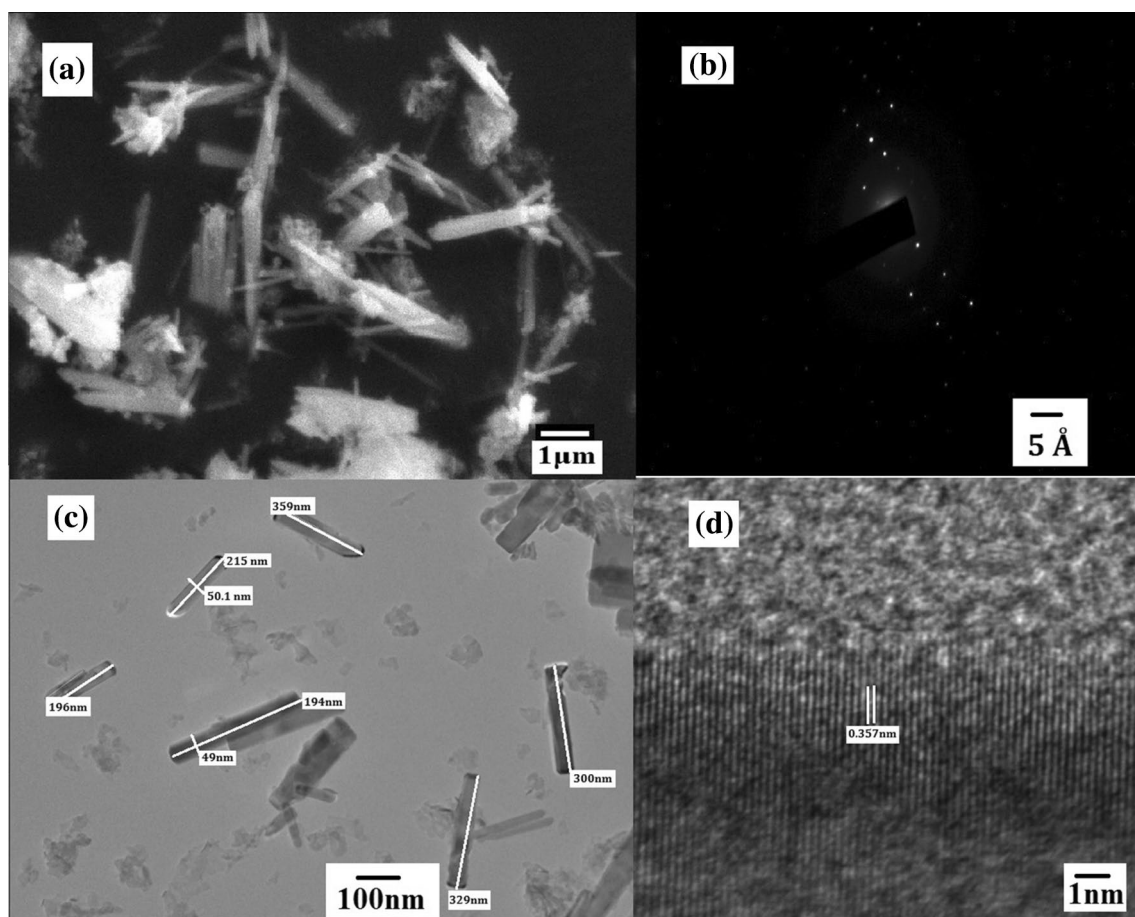

Fig. 2 **a** SEM and **b** SAED pattern **c** TEM and **d** HRTEM images of 10% Tb-doped ZnO nanorods

Fig. 3 EDAX pattern of 10% Tb-doped ZnO nanorods

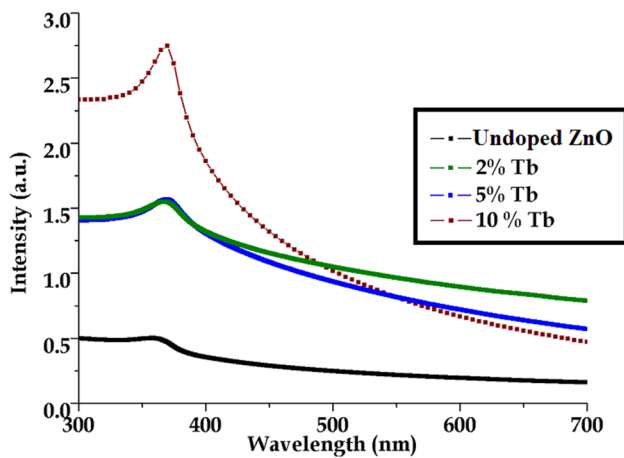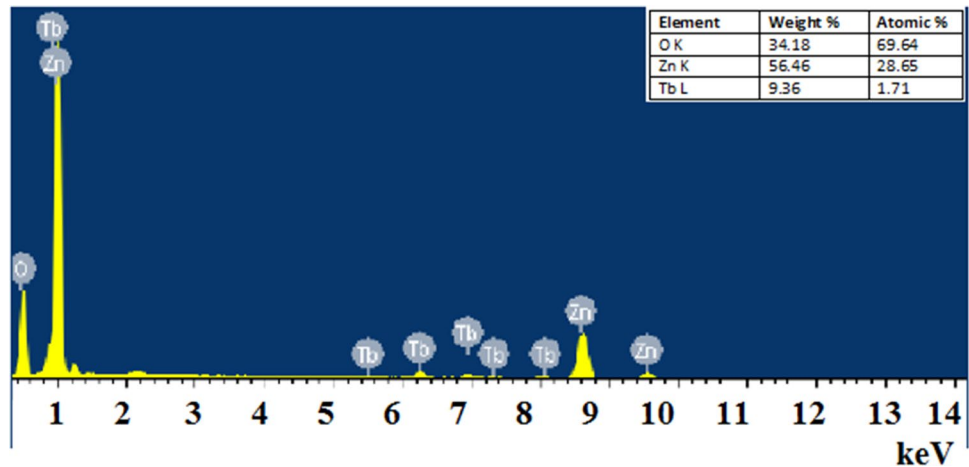| Element	Weight %	Atomic %
O K	34.18	69.64
Zn K	56.46	28.65
Tb L	9.36	1.71

Fig. 4 UV-vis absorption spectra of undoped and Tb (0.02, 0.05, 0.10) doped ZnO nanorods
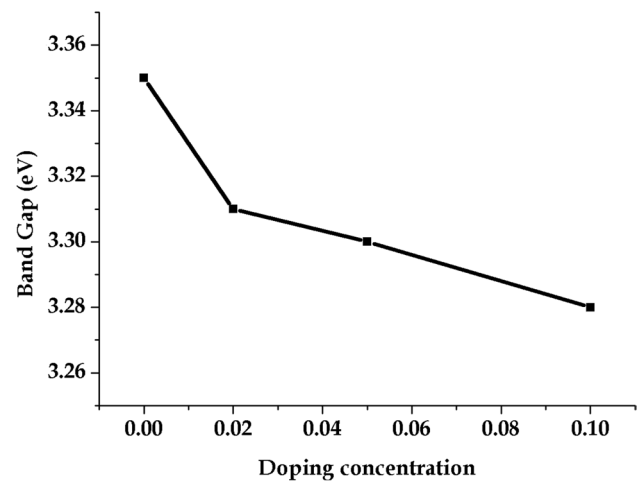

Fig. 5 Band Gap variation of ZnO nanorods as a function of doping concentration

3 Optical study

3.1 UV-vis study

UV-vis absorption spectrum of undoped and Tb-doped ZnO nanorods is shown in Fig. 4. To find the value of band gap Eg, $\lambda_{1/2}$ method has been used;

$$E_g = \frac{hc}{\lambda_{1/2}}$$

where h, is Planck's constant; c, is velocity of light. In this method, the value of absorption band edge wavelength referred as $\lambda_{1/2}$ has been calculated. This band edge wavelength corresponds to 50% wavelength corresponding to excitonic peak [18]. The observed values of band gap are reported in Table 1. It is perceived from Fig. 5 that absorption edge is shifted towards higher wavelength (i.e. band gap decreases) with a rise in dopant concentration. This drop in

band gap value with the corresponding increase in crystallite size indicated the red shift. This observed red shift is attributed to the origin of new levels in the energy band of host ZnO lattice due to introduction of Tb ions. Also the increased sp–f exchange interactions between host ions and dopant ions can lead to decrease in band gap value [19, 20].

3.2 Photoluminescence study

Figure 6 shows room temperature PL spectrum of undoped and Tb-doped ZnO nanorods, recorded at excitation wavelength of 310 nm. PL spectra consist of two main parts: a sharp and intense UV emission (centered at 390 nm) and a weak visible emission [21]. For undoped ZnO nanorods the intensity of peak in UV region is very high but with the incorporation of Tb ions, the intensity of peak has been found to diminish. This decrease in intensity corresponds to decrease in crystalline nature of doped sample, which is
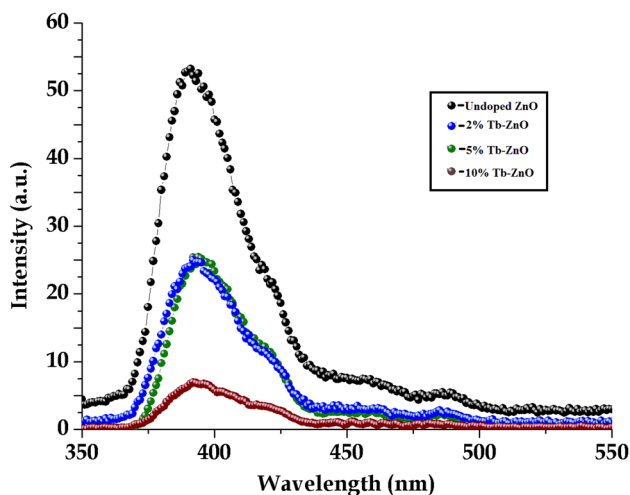
Fig. 6 PL spectra of undoped and Tb (0.02, 0.05, and 0.10)-doped ZnO nanorods

in accordance with XRD results. This sharp UV emission corresponds to near band edge transition whereas visible emissions are due to defect related transitions [22]. The rare earth ions exhibit electron–electron and spin orbit interactions within 4f shell. These d–f transitions are strictly forbidden, as electric dipole transitions in case the rare earth ions occupy the inversion symmetry site in crystal lattice [23].

3.3 Magnetic study

The M-H plots of undoped and Tb-doped ZnO nanorods are given in Fig. 7 and, the observed values of magnetic saturation was reported in Table 1. The undoped ZnO nanorods exhibit ferromagnetic behavior in contrast to diamagnetic behavior of bulk ZnO. The high magnetic moment of Tb
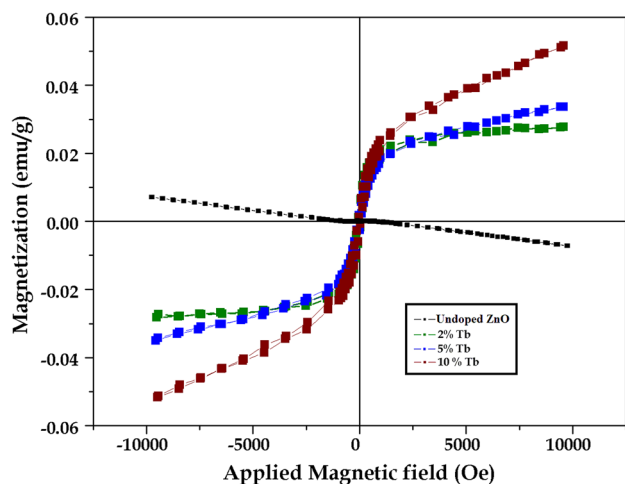
($\sim 9 \mu B$) induces ferromagnetism in ZnO at nanoscale [11]. The random distribution of dopant ion in host ZnO lattice results in weak interaction among ions which lead to the observed ferromagnetism. These interactions depend on the spacing among ions which affects the strength of coupling between Tb^{3+} ions and Zn^{2+} ions [24]. Also, the sp-f exchange interactions can be responsible for the observed ferromagnetism [25]. This observed room temperature ferromagnetism can also be credited to presence of intrinsic defect or oxygen vacancies in the synthesized nanorods [26].

3.4 Electrical study

The effect of various concentrations of Tb as dopant on electrical resistivity of ZnO has been shown in Fig. 8. It is clear from the figure that electrical resistivity of Tb-doped ZnO nanorods is greater than undoped ZnO. This rise in resistivity of doped nanorods is due to decrease in mobility of charge carriers because of the segregation of dopant ions near the grain boundary [27]. Also increase in strain and smaller crystallite size were reported as the probable reason for such increase in resistivity [28]. The increase in dopant concentration gives rise to the generation of defect ions which enables the formation of defect barriers at grain boundary, leading to obstruction to the flow of charge carriers [29]. Thus it can be analyzed form the results that doping concentration plays an important role in tuning the conductivity of the samples.

4 Conclusions

The structural and morphological analyses of Tb-doped ZnO nanorods reveal the formation of well aligned wurtzite structured nanorods without any impurity. Optical study
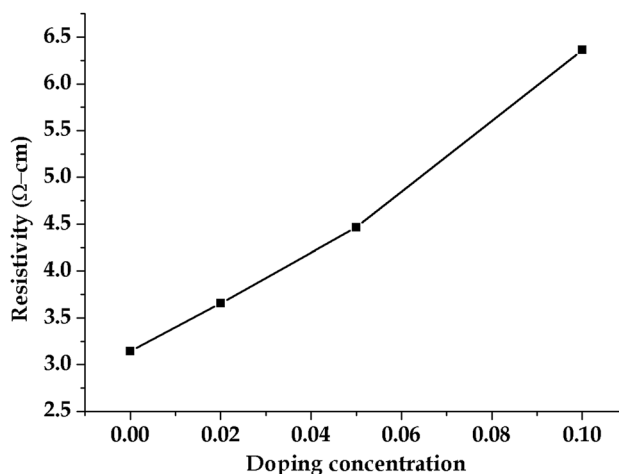

Fig. 7 Magnetization curves of undoped and Tb (0.02, 0.05 and 0.10)-doped ZnO nanorods

Fig. 8 Variation of resistivity with doping concentration

shows that the red shift arises because of some exchange interaction between Tb ions and Zn ions. Sharp UV emission has also been found in photoluminescence study due to near band edge transitions. The magnetic saturation of samples increases with dopant concentration, which confirms Tb-doped ZnO as a suitable candidate for spintronic applications. The increase in value of resistivity with Tb ions suggests the way to control the conductivity of ZnO nanorods.

References

1. Ritu, A simple and effective method for preparation and characterization of zinc oxide. Internation J. Chem. Sci. **11**(2), 1209–1218 (2013)
2. C. Klingshirn, ZnO: from basics towards applications. Phys. Status Solidi (b) **244**(9), 3027–3073 (2007)
3. X. Wang, J. Zhou, J. Song, J. Liu, N. Xu, Z.L. Wang, Piezoelectric field effect transistor and nanoforce sensor based on a single ZnO nanowire. Nano Lett. **6**(12), 2768–2772 (2006)
4. J. Zhang, S. Wang, Y. Wang, M. Xu, H. Xia, S. Zhang, S. Wu, ZnO hollow spheres: preparation, characterization, and gas sensing properties. Sens. Actuators B **139**(2), 411–417 (2009)
5. P.U. Aparna, N.K. Divya, P.P. Pradyumnan, Structural and dielectric studies of Gd doped ZnO nanocrystals at room temperature. J.Mater. Sci. Chem. Eng. **4**(02), 79 (2016)
6. U. Godavarti, V.D. Mote, M. Dasari, Role of cobalt doping on the electrical conductivity of ZnO nanoparticles. J. Asian Ceram. Soc. **5**(4), 391–396 (2017)
7. N. Aggarwal, K. Kaur, A. Vasishth, N.K. Verma, Structural, optical and magnetic properties of Gadolinium-doped ZnO nanoparticles. J. Mater. Sci. Mater. Electron. **27**(12), 13006–13011 (2016)
8. K. Omri, J. El Ghoul, O.M. Lemine, B. Bououdina, B. Zhang, L. El, Mir, Superlattices and microstructures magnetic and optical properties of manganese doped ZnO nanoparticles synthesized by sol–gel technique. Superlattices Microstruct. **60**, 139–147 (2013)
9. N. Srinatha, B. Angadi, K.G.M. Nair, N.G. Deshpande, Y.C. Shao, W. Pong, Journal of electron spectroscopy and spectroscopic investigation of an intrinsic room temperature ferromagnetism in Co doped ZnO nanoparticles. J. Electron Spectros. Relat. Phenomena **195**, 179–184 (2014)
10. C.J. Cong, J.H. Hong, Q.Y. Liu, L. Liao, K.L. Zhang, Synthesis, structure and ferromagnetic properties of Ni-doped ZnO nanoparticles. Solid State Commun. **138**, 511–515 (2006)
11. G.S. Lotey, J. Singh, N.K. Verma, Room temperature ferromagnetism in Tb-doped ZnO dilute magnetic semiconducting nanoparticles. J. Mater. Sci. Mater. Electron. **24**(9), 3611–3616 (2013)
12. S. Bai, X. Liu, D. Li, S. Chen, R. Luo, A. Chen, Synthesis of ZnO nanorods and its application in NO2 sensors. Sens. Actuators, B **153**(2), 110–116 (2011)
13. N. Aggarwal, A. Vasishth, K. Kaur, N.K. Verma, Role of dysprosium doping on structural, optical, magnetic and electrical properties of ZnO nanorods, J. Supercond. Novel Magn., 1–7 (2018)

14. J. Singh, A. Vasishth, N.K. Verma, Multiferroic properties of Zn_{1-x} Mg x O nanoparticles. J. Supercond. Novel Magn. **28**(10), 3069–3074 (2015)
15. R. Yousefi, J. Beheshtian, S.M. Seyed-Talebi, H.R. Azimi, F. Jamali-Sheini, Experimental and theoretical study of enhanced photocatalytic activity of Mg-doped ZnO NPs and ZnO/rGO nanocomposites. Chem. Asian J. **13**(2), 194-203 (2018)
16. A. Khataee, R.D.C. Soltani, A. Karimi, S.W. Joo, Sonocatalytic degradation of a textile dye over Gd-doped ZnO nanoparticles synthesized through sonochemical process. Ultrason. Sonochem. **23**, 219–230 (2015)
17. A.L. Patterson, The Scherrer formula for X-ray particle size determination. Phys Rev **56**(10), 978 (1939)
18. R. Iordanova, R. Gegova, A. Bachvarova-Nedelcheva, Y. Dimitriev, Sol–gel synthesis of composites in the ternary TiO2–TeO2–B2O3 system. Phys. Chem. Glasses-Eur. J. Glass Sci. Technol. Part B **56**(4), 128–138 (2015)
19. R. Elilarassi, G. Chandrasekaran, Influence of Co-doping on the structural, optical and magnetic properties of ZnO nanoparticles synthesized using auto-combustion method. J. Mater. Sci. Mater. Electron. **24**(1), 96–105 (2013)
20. C. Li, G. Fang, Q. Fu, F. Su, G. Li, X. Wu, X. Zhao, Effect of substrate temperature on the growth and photoluminescence properties of vertically aligned ZnO nanostructures. J. Cryst. Growth **292**(1), 19–25 (2006)
21. A. Hastir, N. Kohli, R.C. Singh, Comparative study on gas sensing properties of rare earth (Tb, Dy and Er) doped ZnO sensor. J. Phys. Chem. Solids **105**, (2017)
22. K. Bandopadhyay, J. Mitra, Zn interstitials and O vacancies responsible for n-type ZnO: what do the emission spectra reveal'. RSC Adv. **5**(30), 23540–23547 (2015)
23. K. Kaur, G.S. Lotey, N.K. Verma, Structural, optical and magnetic properties of cobalt-doped CdS dilute magnetic semiconducting nanorods. Mater. Chem. Phys. **12880**, 6–11 (2013)
24. S. Ramu, R.P. Vijayalakshmi, Effect of terbium doping on the structural and magnetic properties of ZnS nanoparticles. J. Supercond. Nov. Magn. **30**(7), 1921–1925 (2017)
25. J.M.D. Coey, M. Venkatesan, C.B. Fitzgerald, Donor impurity band exchange in dilute ferromagnetic oxides. Nat. Mater. **4**(2), 173–179 (2005)
26. D.R. Kumar, K.S. Ranjith, L.R. Nivedita, R.T.R. Kumar, Effect of samarium doping on structural, optical and magnetic properties of vertically aligned ZnO nanorod arrays. J. Rare Earths **35**(10), 1002–1007 (2017)
27. H.M. Zhou, D.Q. Yi, Z.M. Yu, L.R. Xiao, J. Li, Preparation of aluminum doped zinc oxide films and the study of their microstructure, electrical and optical properties. Thin Solid Films **515**(17), 6909–6914 (2007)
28. R. Ghosh, D. Basak, S. Fujihara, Effect of substrate-induced strain on the structural, electrical, and optical properties of polycrystalline ZnO thin films. J. Appl. Phys. **96**, 2689–2692 (2004)
29. N.K. Divya, P.U. Aparna, P.P. Pradyumnan, Dielectric Properties of Er 3 + Doped ZnO Nanocrystals. Adv. Mater. Phys. Chem. **5**(8):287 (2015)